Cu$_x$Ir$_{1−x}$ Nanoalloy Catalysts Achieve Near 100% Selectivity for Aqueous Nitrite Reduction to NH$_3$

Hao Li,[||] Chenxu Yan,[||] Hongyu Guo,[||] Kihyun Shin, Simon M. Humphrey,* Charles J. Werth,* and Graeme Henkelman*

ACCESS | ⬛ Metrics & More | 📰 Article Recommendations | 🆂�Ⓘ Supporting Information

ABSTRACT: Nitrite (NO$_2^-$) is an abundant contaminant in nature that threatens human health. A catalytic process that converts NO$_2^-$ to less harmful products has been proven to be an effective strategy for NO$_2^-$ removal. Most previous studies, however, targeted selectivity toward N$_2$ using Pd catalysts, which severely limits the potential for the recovery of value-added byproducts from the catalytic process. Here, we report experimental and theoretical evidence that both Ir and Cu$_x$Ir$_{(100−x)}$ nanoparticles possess near 100% NH$_3$ selectivity for NO$_2^-$ reduction compared to the <1% NH$_3$ selectivity achieved by nano-Pd. These NH$_3$-selective catalysts could be useful for both water purification and ammonia production.

Active and 100% NH$_3$-Selective Catalysts

KEYWORDS: *nitrite reduction, iridium, ammonia selectivity, density functional theory, Cu−Ir alloy, nanoparticles*
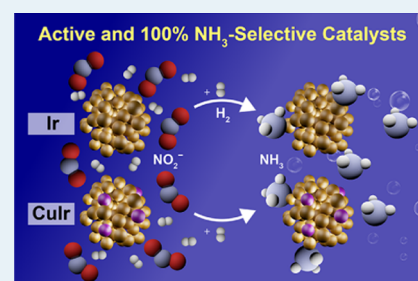
Nitrite (NO$_2^-$) is a harmful contaminant widely found in water and soil.[1−3] Anthropogenic sources of NO$_2^-$ accumulate in crops and other foods and in drinking water. Ingestion of NO$_2^-$ leads to the generation of *N*-nitrosamine byproducts, which are proven carcinogens and also damage hemoglobin, leading to cellular degradation and even brain damage in infants.[4,5] Many countries, therefore, have strict regulations on the maximum NO$_2^-$ level in drinking water. However, few cost-effective methods have been identified thus far to effectively abate NO$_2^-$ contamination on an industrial scale.

Catalytic reduction has proven to be a powerful strategy for denitrification in water.[6] Compared to conventional NO$_2^-$ removal methods (e.g., ion exchange[7]), catalytic degradation holds a number of significant advantages including less secondary waste, shorter industrial-scale startup times, lower overall energy consumption, and higher NO$_2^-$ removal efficiency.[6,8,9] However, given the complicated reaction network of nitrite reduction (Figure 1), the design and scalable synthesis of NO$_2^-$ reduction catalysts presents a major and as-yet unsolved challenge.[6]

In recent years, several studies have reported effective NO$_2^-$ reduction catalysts for water treatment (Table 1). For example, Seraj et al. showed that PdAu alloy nanoparticles (NPs) have enhanced nitrite reduction activity as compared to pure PdNPs.[8] Qian et al. found that Pd precursors directly reduced on pure AuNPs had a much greater activity per gram of Pd for NO$_2^-$ reduction.[10] Recently, a combined theoretical and experimental strategy was employed by our group to design a series of bimetallic core@shell structures (e.g., Au@Pd) that led to a high density of optimized reaction sites on the NP surfaces, leading to a corresponding enhancement in NO$_2^-$

reduction activity.[9] Until now, Pd-based NPs have been the most commonly studied catalysts for NO$_2^-$ reduction due to their high activities and selectivities toward dinitrogen (N$_2$) formation, as observed in both experiments[8,10,11] and calculations[9,12] (Table 1).

In contrast, only a handful of studies have targeted the selectivity of nitrite reduction toward ammonia (NH$_3$),[13,14] primarily because of its environmental and human health toxicity (Table 1).[6] Yet, NH$_3$ is also a crucial precursor to fertilizer production for agriculture (i.e., the Haber−Bosch process[15]); NH$_3$ is also an emerging energy storage material for use in fuel cell technologies.[16−18] Haber−Bosch plants are notoriously energy-intensive, utilizing 1% of total global energy to achieve the necessarily forcing reaction conditions (i.e., T ∼ 450 °C and p ∼ 300 bar).[19] Alternative NH$_3$ production methods could therefore greatly help to produce this valuable product from waste streams. To the best of our knowledge, no prior studies have reported non-Pd-based catalysts that select almost exclusively for NH$_3$. One exception is work on electrocatalytic nitrate/nitrite reduction, which has emerged as a promising process for NH$_3$ production with the goal of using electricity supplied by renewable energy such as solar and wind to achieve on-demand production of fertilizers.[20,21] However, since the hydrogen evolution reaction (HER) is
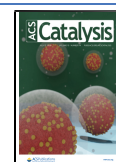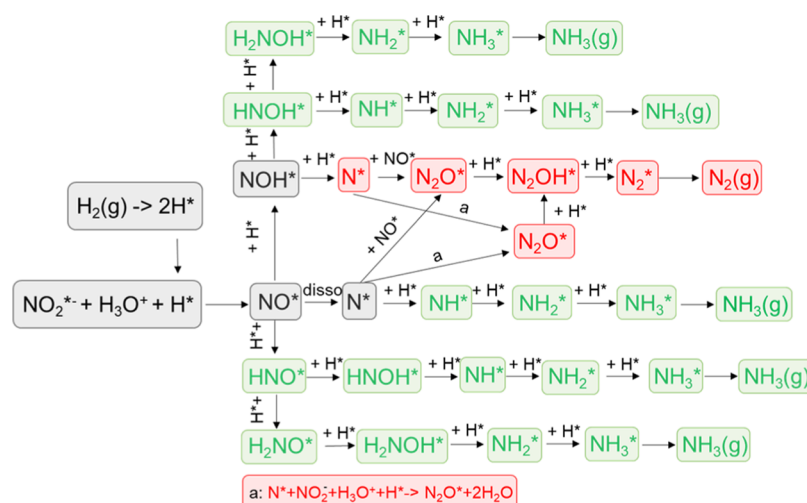
Figure 1. Catalytic reaction pathways for nitrite reduction with hydrogen gas as the reducing agent. The formation of water in the reactions is not shown.

Table 1. Summary of Nitrite Reduction Catalysts Reported in Recent Years

catalyst	activity	NH_3 selectivity	temperature	references
AuNPs (∼4.4 nm)	not active	N/A	22 ± 1 °C	Seraj et al.[8]
PdNPs (∼14.8 nm)	1.99 L g_{metal}^{-1} min^{-1}	<2%	22 ± 1 °C	Seraj et al.[8]
$Pd_{53}Au_{47}$ NPs[a] (∼2.2 nm)	5.12 L g_{metal}^{-1} min^{-1}	<2%	22 ± 1 °C	Seraj et al.[8]
$Pd_{80}Cu_{20}$ colloids (∼5.0 nm)	9.8 L $mmol^{-1}$ M^{-1} h^{-1}	0.8%	room temperature	Guy et al.[11]
80 sc% Pd-on-AuNPs (∼4.3 nm)	576 L g_{Pd}^{-1} min^{-1}	0.4%	N/A	Qian et al.[10]
$Au@Pd_{monolayer}$ NPs (∼4.4 nm)	246 L $g_{surface\ Pd}^{-1}$ min^{-1}	2.5%	room temperature	Li et al.[9]
Pd@MIL-101[b] (∼2.4 nm)	1.252 $mg^{0.3}$ $L^{-0.3}$ min^{-1}	7.48%	room temperature	Zhang et al.[13]
Pd−ethanol@MIL-101[c]	0.894 $mg^{0.3}$ $L^{-0.3}$ min^{-1}	0.31%	room temperature	Zhang et al.[13]
Pd−1-dodecanethiol@MIL-101[d]	0.546 $mg^{0.3}$ $L^{-0.3}$ min^{-1}	10.18%	room temperature	Zhang et al.[13]
CNFs/Ni[e]	N/A	∼70%	room temperature	Espinosa and Lefferts[14]
Rh/Al_2O_3[f]	∼3−24 L $g_{surface\ metal}^{-1}$ min^{-1}	∼68−95%	room temperature	Clark et al.[23]

[a]Composition measured from inductively coupled plasma optical emission spectrometry (ICP-OES). [b]PdNPs prepared on a type of metal−organic framework (MIL-101). [c]Pd@MIL-101 chelated with ethanol. [d]Pd@MIL-101 chelated with 1-dodecanethiol. [e]Carbon nanofibers (CNFs) grown on the surface of polycrystalline Ni foam. [f]Commercial Rh/Al_2O_3 in a solution with pH measured from 7.5 to 11.5.

more facile than electrochemical nitrate/nitrite reduction, H_2 gas is lost from these reactors and the Faradic efficiencies are low; as a result, this process has not yet met the requirements for industrial-scale applications.[22] Another exception is a recently developed Rh/Al_2O_3 catalyst, but it was only evaluated at pH = 11.5.[23] Higher pH favors NH_3 selectivity due to competitive adsorption of OH^- over nitrite that lowers the N:H ratio on the catalyst surface, making N−N pairing less likely and therefore selecting toward NH_3.[24] Additionally, the use of an Al_2O_3 support could also contribute to the NH_3 selectivity.[25] Therefore, alternative heterogeneous catalysts that can selectively form NH_3 from NO_2^- at near-circumneutral pH with high H_2 gas utilization are currently unknown and have not been investigated in detail.

Considering the aforementioned limitations of current NH_3 synthesis methods and the abundance of NO_2^- and its parent compound NO_3^- in the environment, we are motivated to discover new nitrite reduction catalysts that favor NH_3 over N_2 formation to treat agricultural run-off or groundwater affected by this run-off for ammonia recovery as fertilizer. Although nitrite concentration in these streams might be too low for an economical direct treatment,[26−29] a selective catalyst that converts NO_2^- to NH_3 could be valuable in a two-stage catalytic process that converts the more abundant parent compound NO_3^- to NO_2^- in the first stage and selectively

reduces nitrite to ammonia for recovery in the second stage.[30] The NH_3 selective catalyst with the two-stage process could be even more useful to treat high nitrate/nitrite waste brine from current state-of-the-art technologies for nitrate and nitrite removal (e.g., ion exchange and reverse osmosis), which are costly to dispose of.[31] This process would simultaneously alleviate NO_2^- contamination and reduce the cost of agricultural fertilizer and brine disposal. In a previous combined theoretical and experimental study, Shin et al.[12] proposed a catalyst design guideline; they suggested that higher NO_2^- concentration promotes selectivity toward N_2, whereas a facile supply of H_2 favors selectivity toward NH_3 formation. Inspired by this hypothesis, we have undertaken a systematic search for new nanocatalysts with high H coverages, which should favor NH_3 production from aqueous NO_2^-. Using a volcano activity model to represent NO_2^- reduction toward NH_3 selectivity as a function of catalyst-reagent binding strength, we theoretically identified a number of potential NH_3-selective catalysts from a range of transition-metal surfaces that achieve high NO_2^- reduction activities and correspondingly high H-coverage at workable H_2 pressures.

More specifically, we have employed density functional theory (DFT) calculations to generate a catalytic model to estimate the activity of NO_2^- reduction toward NH_3, where the relative NH_3 selectivity was derived using N and NH_3
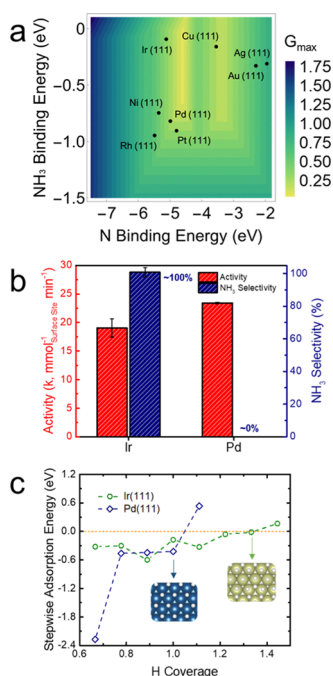
Figure 2. (a) Volcano activity plot for nitrite reduction through the NH_3 formation pathway with the close-packed monometallic surfaces indicated (black marks). (b) Nitrite reduction activities and their NH_3 selectivities on pure Pd and IrNPs. The measured selectivity that is slightly higher than 100% was due to statistical uncertainty in the measurements of the NO_2^- and NH_3 components. (c) Calculated stepwise adsorption energy of H on Pd and Ir(111) surfaces. Insets show the saturated H adsorption on the surfaces. Blue, yellow, and white spheres represent Pd, Ir, and H, respectively. More computational and experimental details can be found in the Supporting Information.

binding energies at the catalytic surfaces as reactivity descriptors (Figure 2a).[9] Based on linear scaling realtionships[32] between the binding energies of N and other adsorbates (e.g., HNO* and NH*) in this reaction network, it was found that all binding energies of reaction intermediates can be estimated through linear relationships with the N binding energy. Therefore, the reaction free energies can be estimated using the N and NH_3 binding energies together with linear relationships between the binding energy of N and the other relevant adsorbates.[9] The two peaks found in the volcano plot represent the highest theoretical activity of two pathways (i.e., those with the lowest estimated reaction free energies): the left peak corresponds to the NH_3 formation through a NO dissociative pathway, while the right peak corresponds to the NO associative pathways where the activation of the N−O bond occurs after NO hydrogenation (Figure 1). Note that the volcano plot of N_2 formation selectivity has the same trend as the NH_3 selectivity volcano,[9] due to the fact that both reactions have the same rate-determining step. Additionally, we note that considering the transition states and reaction kinetics in the model can help to acquire a more precise volcano activity plot. However, due to the high computation cost of the energy barrier calculations for nitrite reduction with such a complicated reaction network, and the proven predictive power of the use of reaction free energy for evaluating nitrite reduction activity,[8,9,11,12,33] the use of reaction free energy is expected to provide an inexpensive descriptor for nitrite reduction catalyst design. By adding the calculated N and NH_3

binding energies of the catalysts on to the volcano plot, we found that some monometallic catalysts have promising NO_2^- reduction activities that are close to one of the volcano peaks. It can be clearly seen that, in addition to the well-studied Pd catalysts, there are other promising candidates, such as Ir, that should also have high activities for NO_2^- reduction, as they are also close to the volcano peak. It should be noted that this volcano model was not used to predict the competing product selectivities between NH_3 and N_2 due to a lack of information about the complicated coadsorbate coverage. Instead, the reaction selectivities here are evaluated independently using the models developed by Shin et al.[12] Specifically, compared to Pd, Ir has 5d electrons that were found to give rise to different hydrogen adsorption properties on the surface;[9,34,35] thus, we expect that this difference should lead to a different selectivity in nitrite reduction. To test these predictions, we then used experiments to validate the predictions (*vide infra*).

Based on the predictions gleaned from the volcano model, we first prepared monometallic IrNPs and PdNPs with a similar size (~2 nm) and supported them on amorphous silica (a-SiO_2) for use in model batch NO_2^- reduction experiments. To do so, a 0.1 M phosphate buffer solution (pH = 6.4 ± 0.1) containing 1.25 g L^{-1} catalyst in a sealed, well-mixed serum bottle was purged with H_2 at 120 cm^3 min^{-1} for 1 h. Next, a small aliquot of nitrite stock solution was spiked into the serum bottle to start the reaction and samples were taken regularly for the analysis of NO_2^- and NH_3 concentrations using ion chromatography and Hach colorimetric kits. The apparent pseudo-first-order rate constants were obtained from the slopes of the linear regression of the natural log of NO_2^- concentration versus time plots for up to 80% NO_2^- conversion. The data were then normalized to the number of surface metal atoms in each catalyst (using transmission electron microscopy (TEM) data and assuming all NPs have a cuboctahedral shape). The resulting NH_3 selectivity was defined as the percentage of reduced NO_2^- that was converted to NH_3. The experimental activity (red bars) and NH_3 selectivity (blue bars) for both IrNPs and PdNPs are shown in Figure 2b. The NO_2^- reduction activity of IrNPs was 19.1 $mmol_{surface\ atom}^{-1}$ min^{-1}, similar to that of PdNPs (23.5 $mmol_{surface\ atom}^{-1}$ min^{-1}). Excitingly, however, despite the close activities of the two metal NPs, the IrNPs exhibited ~100% selectivity toward NH_3 while the NH_3 selectivity of PdNPs was negligible and below the detection limit of the analytical method used (<0.07%). The slightly higher overall reduction activity of the PdNPs compared to the IrNPs is in good agreement with the theoretical predictions from the volcano model (Figure 2a). TEM images of the as-prepared catalysts indicated a homogeneous distribution of NPs on the a-SiO_2 support (Figure S1). The IrNPs and PdNPs were all found to be approximately cuboctahedral in shape with narrow size distributions (1.7 ± 0.2 nm (Ir); 2.4 ± 0.5 nm (Pd)) (Figure S2). The slight size difference between the IrNPs and PdNPs originated from an intrinsic difficulty to obtain larger IrNPs,[35−37] but the normalized activities shown in Figure 2b reflect the surface to bulk atom ratio, providing qualitatively comparable trends between Ir and Pd. We also attempted to alter the H_2 flow rates and the initial concentration of NO_2^- in the reduction experiments using both Ir and Pd catalysts; only significantly lower initial NO_2^- concentrations were found to improve the NH_3 selectivity on PdNPs (e.g., an initial NO_2^- concentration of 10 ppm led to an NH_3 selectivity of ca. 2.3%). This result is in good agreement with our expectation that

lowering the NO_2^- concentration promotes NH_3 selectivity due to a higher coverage of hydrogen on the surface.

The theory proposed by Shin et al. indicates that a higher H-coverage promotes NH_3 selectivity by providing a higher chance of hydrogenation reactions (Figure 1).[12] To understand the significantly higher NH_3 selectivity on IrNPs compared to PdNPs observed in our work, we evaluated the relative H-coverage on different catalysts by calculating stepwise adsorption energies of H on the Ir(111) and Pd(111) surfaces (Figure 2c, with the calculation methods described in the Supporting Information).[38] It can be seen that the theoretical maximum H-coverage (the coverage before the stepwise adsorption energy becomes greater than zero) of Ir(111) is ~1.3, which is higher than that of Pd(111) (= 1). This indicates that Ir(111) can thermodynamically accommodate more H on the surface than Pd(111).[39] These results can be further generalized with our previous conclusions: 5d transition metals have larger orbitals compared to 4d transition metals,[40] which leads to stronger interactions with H and correspondingly higher theoretical H surface coverages under ambient conditions.[35,41] This qualitatively explains why PdNPs have slightly better activity for NO_2^- reduction as shown on the volcano plot (Figure 2a) because IrNPs have higher NH_3 selectivity due to the stronger capacity of accommodating H on the catalyst surfaces. This also helps to explain why other 5d transition-metal catalysts such as Pt also have relatively high NH_3 selectivity, as found in previous studies.[42,43] Although the hydrogen coverages at both Pd and Ir(111) appear relatively high, these calculations are done without considering the competition of other adsorbates. According to our previous calculations,[9] N and many N-related species of nitrite reduction have stronger binding strengths than H. Therefore, the actual coverage of H will be significantly lower when the nitrite reduction reaction reaches equilibrium; the trend, however, is not expected to change. These results are in good agreement with our previous combined experimental and computational study that the slightly higher H-coverage on 5d transition metal leads to significantly different hydrogenation activity, as compared to 4d transition metals.[34] Additionally, as shown in the previous results by Shin et al.,[12] a minor increase in the hydrogen supply can significantly improve the NH_3 selectivity in experiments. Based on these results, and given the fact that the H-coverage on Ir(111) is >30% higher than that on Pd(111), we consider this is a significant difference in the hydrogen accommodation capacity that contributes to the observed difference in the resulting NH_3 selectivity. It should be noted that there are other factors that could be used to tune the NO_2^- reduction selectivity including the use of an active support/substrate or increasing the solution pH.[24,44,45] Notably, some previous studies have shown that NH_3 selectivity increases with a higher solution pH.[23] A pH higher than the pH_{ZPC} (ZPC = zero point of charge) of the metallic surface will promote a negatively charged catalyst surface, resulting in electrostatic repulsion of NO_3^- and NO_2^- ions and therefore a higher H:N ratio on the catalytic surface that favors NH_3 formation.[24,44] Despite the fact that NH_3 selectivity can be improved by raising the solution pH, to the best of our knowledge, the IrNP catalyst is the only current example to have achieved near 100% NH_3 selectivity for nitrite reduction under very mildly acidic conditions (pH = 6.4 ± 0.1). Such a moderate pH is environmentally relevant, meaning that the IrNPs could operate effectively under realistic conditions while

achieving NH_3 selectivity values that are superior to other NO_2^- reduction catalysts.

Since IrNPs were found to be highly selective toward NH_3 formation, we then performed similar batch kinetics experiments for nitrite reduction using as-synthesized $Cu_xIr_{(100-x)}$ alloy NPs. Ir-based alloys, especially those containing earth-abundant 3d metals, are attractive for several reasons: (a) alloying cheaper Cu with Ir can reduce the overall dependence on Ir; (b) from a theoretical perspective, a theoretical line joining Cu and Ir in the volcano plot in Figure 2a is found to cross the volcano peak, which suggests that homogeneous Cu—Ir alloys (i.e., solid solutions) can further tune the binding energies of N and NH_3 and also the catalytic activity of the alloy (Figure S3),[8,9,11,46] (c) alloying more noble and therefore less reactive metals (e.g., Cu, Ag, and Au) with more reactive metals can reduce sulfur poisoning in practical water treatment due to beneficial atomic ensemble effects (Figure S4);[8,41,47] and, (d) Ir-based alloy catalysts are rarely explored because many are only accessible as metastable structures on the nanoscale.[35,36] Here, bimetallic $Cu_xIr_{(100-x)}$ NPs with various target compositions (x = 10, 25, and 50) were prepared using our previously developed methods.[37] The alloy $Cu_xIr_{(100-x)}$ NPs were deposited on a-SiO_2, and their catalytic activities for nitrite reduction were measured. Powder X-ray diffraction (PXRD) patterns confirmed the random solid-solution structure of the alloy NPs, as the reflections showed a consistent shift to a higher angle with an increasing Cu content (Figure 3a). Further, 2D energy-dispersive spectroscopy (EDS) mapping of the NPs showed a homogeneous distribution of Cu and Ir across the NPs.[37] The actual
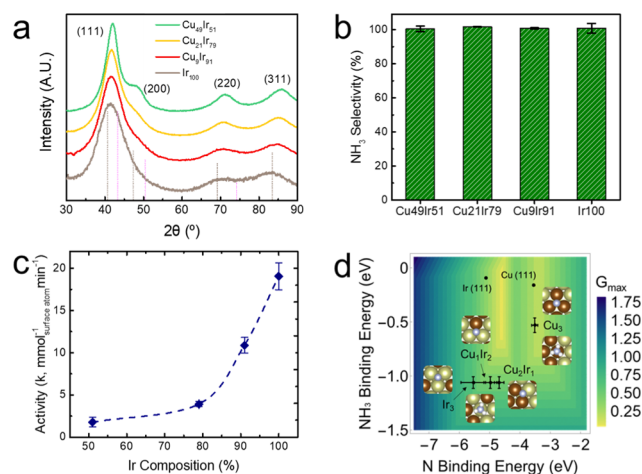

Figure 3. (a) PXRD patterns of $Cu_xIr_{(100-x)}$ alloy NPs with different compositions. The theoretical reflection positions of Cu (pink dash lines, JCPDS card # 04-0836) and Ir (brown dash lines, JCPDS card # 006-0598) are shown for reference. (b) NH_3 selectivity and (c) measured reaction rate constants of nitrite reduction on $Cu_xIr_{(100-x)}$ NPs. The measured selectivity slightly higher than 100% was due to uncertainties in the measurements of the NO_2^- and NH_3 contents. (d) Volcano activity plot for nitrite reduction through the NH_3 formation pathways, with points indicating Ir(111), Cu(111), and the four triatomic ensembles (Ir_3, Cu_1Ir_2, Cu_2Ir_1, and Cu_3) sampled on more than 15 randomly generated alloyed $Cu_{25}Ir_{75}$(111) surfaces. The error bars indicate the standard deviation of adsorption energies calculated from 10 binding sites. Insets show the adsorption geometries of N and NH_3 at typical binding sites. Teal, brown, white, and blue spheres represent Ir, Cu, H, and N, respectively. Calculations on other Cu—Ir compositions can be found in Figure S9.

composition of the as-synthesized alloy NPs was found to be close to the nominal ratio, as indicated by inductively coupled plasma optical emission spectroscopy of bulk samples (ICP-OES) (Table S1). Corresponding TEM images showed that the alloy NPs have an average size of around 2 nm, similar to the monometallic IrNPs (Figure S5). It should be noted that Cu is more easily oxidized by atmospheric oxygen during synthesis and storage, since the standard reduction potential of Cu^{2+}/Cu^0 (0.34 V) is much lower than that of Ir^{3+}/Ir^0 (1.16 V).[48] A combined Cu 2p X-ray photoelectron spectroscopy (XPS) spectrum and Cu LMM Auger spectrum confirmed that the majority (~74%) of the copper was in the metallic state, with slight (~26%) Cu(II) oxide on the surface (Figure S6). Using similar catalytic tests as described above for the PdNPs and IrNPs, the $Cu_xIr_{(100-x)}$ NPs showed a NH_3 selectivity of ~100% (Figure 3b). Surprisingly, instead of having improved activities, our experimental results show that alloying Cu into Ir leads to a monotonic decrease in the activity (Figure 3c). For example, the activity of pure IrNPs was about five times the activity of $Cu_{49}Ir_{51}$ NPs (19.06 $mmol_{surface\ atom}^{-1}\ min^{-1}$ vs 3.92 $mmol_{surface\ atom}^{-1}\ min^{-1}$). Using DFT calculations, the activity trends found on the $Cu_xIr_{(100-x)}$ NPs could be adequately explained by the volcano activity plots with the calculated average N and NH_3 binding energies at different triatomic ensembles on the alloyed $Cu_xIr_{(100-x)}$ surfaces: although the N binding energy is tunable with the increased ratio of Ir in a triatomic ensemble, the average binding of NH_3 is not altered on the Ir sites of $Cu_xIr_{(100-x)}$ surfaces, since NH_3 is adsorbed at Ir-atop sites instead of at threefold hollow sites (Figure 3d, inset).[9,49] Due to the significant electronic and strain effects induced in the Cu–Ir alloys,[41,47,50,51] NH_3 tends to become overbound at Ir-atop sites, which in turn breaks the well-known scaling relationship of adsorbates on transition-metal surfaces[52] and leads to lower activities on the $Cu_xIr_{(100-x)}$ alloy NPs. This effect of alloying can be further evaluated by the projected density of states (PDOS) of d-electrons of the surface Ir sites and the observed up-shift of the calculated d-band center (average energy of d-electrons)[53] after alloying (Figure S7). According to the d-band center theory,[53] an up-shift of d-band center pushes more antibonding states above the Fermi level, which in turn strengthens the NH_3 binding. These results are similar to our previous studies on PtAu and AgIr alloy NPs for hydrogenation:[34,35] although the line between Pt and Au (or Ir and Ag) on the C=C hydrogenation volcano plot goes across the volcano peak, alloying Au into Pt (or Ag into Ir) does not lead to an improved performance for C=C hydrogenation since their binding energy descriptors at the alloyed ensembles are located far from the volcano peak, which in turn leads to lower activity with the increased ratio of inert metallics.[34,41] Meanwhile, as Cu–Ir was found to be less tunable for H adsorption on Ir-related sites due to the intrinsic properties on the active 5d transition metals (Figure S8),[37] the H-coverage at those Ir sites of the alloys are expected to remain similar to that of Ir(111), leading to the superior NH_3 selectivity similar to pure IrNPs (Figure 2).

To generalize our conclusions and enable further useful structure-function predictions, we also screened the surface alloys of some other inert metallic surfaces (Cu, Ag, and Au(111)) doped with catalytically active 5d transition metals included in Figure 2a (Ir and Pt) (Figure 4). It can be clearly seen that alloying Ir on an inert surface leads to overbinding of NH_3 at the Ir-atop site, resulting in a low nitrite conversion rate. However, some of the Pt-based alloys show good activity,
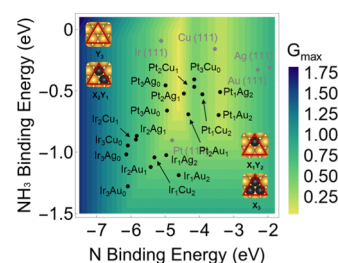

Figure 4. Volcano activity plot for nitrite reduction through the NH_3 formation pathways, with triatomic ensembles (Y_3, X_1Y_2, X_2Y_1, and X_3, X = Ir and Pt and Y = Cu, Au, and Ag) of the surface alloys on Y (111). The X_1Y_2, X_2Y_1, and X_3 triatomic ensembles were modeled as an X (111) surface, respectively, replaced by 1, 2 (twofold), and 3 (threefold) X atoms. Insets show the surface alloy models considered for the calculations: yellow and black spheres represent the Y and X atoms, respectively. The red triangles represent the triatomic ensembles as the binding sites.

with their binding energies at the triatomic ensembles close to the volcano peak. In addition to the Ir-based catalysts, other active 5d transition metals including Pt are also expected to have good NH_3 selectivity.[42,43] Due to the predicted high activity of Pt alloys from the volcano model (Figure 4), we predict that alloying Pt and other inert transition metal (e.g., Ag) could guarantee both high activity for NO_2^- reduction and a promising NH_3 selectivity.

In summary, we report that pure IrNPs and alloyed $Cu_xIr_{(100-x)}$ NPs possess outstanding NH_3 selectivity (~100%) for aqueous nitrite reduction in a near-neutral pH solution. Additionally, pure IrNPs are found to have a nitrite reduction activity that is close to PdNPs, which are used industrially. Compared to those N_2-selective catalysts including Pd and Pd alloys, we expect that the use of the NH_3-selective catalysts can help to expand the potential applications of NO_2^- removal as well as in NH_3 production.

■ ASSOCIATED CONTENT

ⓈI Supporting Information

The Supporting Information is available free of charge at https://pubs.acs.org/doi/10.1021/acscatal.0c01604.

> Detailed computational, modeling, and experimental methods and additional computational, catalytic, and characterization results (PDF)

■ AUTHOR INFORMATION

Corresponding Authors

Simon M. Humphrey − Department of Chemistry, The University of Texas at Austin, Austin, Texas 78712, United States; ⊙ orcid.org/0000-0001-5379-4623; Email: smh@cm.utexas.edu

Charles J. Werth − Department of Civil, Architectural and Environmental Engineering, The University of Texas at Austin, Austin, Texas 78712, United States; ⊙ orcid.org/0000-0002-8492-5523; Email: werth@utexas.edu

Graeme Henkelman − Department of Chemistry and The Oden Institute for Computational Engineering and Sciences, The University of Texas at Austin, Austin, Texas 78712, United States; ⊙ orcid.org/0000-0002-0336-7153; Email: henkelman@utexas.edu

Authors

Hao Li − *Department of Chemistry and The Oden Institute for Computational Engineering and Sciences, The University of Texas at Austin, Austin, Texas 78712, United States*

Chenxu Yan − *Department of Civil, Architectural and Environmental Engineering, The University of Texas at Austin, Austin, Texas 78712, United States;* orcid.org/0000-0002-2227-5510

Hongyu Guo − *Department of Chemistry, The University of Texas at Austin, Austin, Texas 78712, United States*

Kihyun Shin − *Department of Chemistry, The University of Texas at Austin, Austin, Texas 78712, United States;* orcid.org/0000-0002-1748-8773

Complete contact information is available at:
https://pubs.acs.org/10.1021/acscatal.0c01604

Author Contributions

‖H.L., C.Y., and H.G. contributed equally to this work.

Notes

The authors declare no competing financial interest.

■ REFERENCES

(1) Elmi, A. A.; Madramootoo, C.; Egeh, M.; Hamel, C. Water and Fertilizer Nitrogen Management to Minimize Nitrate Pollution from a Cropped Soil in Southwestern Quebec, Canada. *Water, Air, Soil Pollut.* **2004**, *151*, 117−134.

(2) Pye, V. I.; Patrick, R. Ground Water Contamination in the United States. *Science* **1983**, 713−718.

(3) Zhu, X.; Zeng, X. C.; Chen, X.; Wu, W.; Wang, Y. Inhibitory Effect of Nitrate/Nitrite on the Microbial Reductive Dissolution of Arsenic and Iron from Soils into Pore Water. *Ecotoxicology* **2019**, *28*, 528−538.

(4) Weyer, P. J.; Cerhan, J. R.; Kross, B. C.; Hallberg, G. R.; Kantamneni, J.; Breuer, G.; Jones, M. P.; Zheng, W.; Lynch, C. F. Municipal Drinking Water Nitrate Level and Cancer Risk in Older Women: The Iowa Women's Health Study. *Epidemiology* **2001**, *12*, 327−338.

(5) Tamme, T.; Reinik, M.; Roasto, M. Nitrates and Nitrites in Vegetables: Occurrence and Health Risks. In *Bioactive Foods in Promoting Health*; Academic Press, 2010; pp 307−321.

(6) Yin, Y. B.; Guo, S.; Heck, K. N.; Clark, C. A.; Coonrod, C. L.; Wong, M. S. Treating Water by Degrading Oxyanions Using Metallic Nanostructures. *ACS Sustainable Chem. Eng.* **2018**, *6*, 11160−11175.

(7) Kapoor, A.; Viraraghavan, T. Nitrate Removal From Drinking Water. *J. Environ. Eng.* **1997**, *123*, 371−380.

(8) Seraj, S.; Kunal, P.; Li, H.; Henkelman, G.; Humphrey, S. M.; Werth, C. J. PdAu Alloy Nanoparticle Catalysts: Effective Candidates for Nitrite Reduction in Water. *ACS Catal.* **2017**, *7*, 3268−3276.

(9) Li, H.; Guo, S.; Shin, K.; Henkelman, G.; Wong, M. S. Design of a Pd-Au Nitrite Reduction Catalyst by Identifying and Optimizing Active Ensembles. *ACS Catal.* **2019**, *9*, 7957−7966.

(10) Qian, H.; Zhao, Z.; Velazquez, J. C.; Pretzer, L. A.; Heck, K. N.; Wong, M. S. Supporting Palladium Metal on Gold Nanoparticles Improves Its Catalysis for Nitrite Reduction. *Nanoscale* **2014**, *6*, 358−364.

(11) Guy, K. A.; Xu, H.; Yang, J. C.; Werth, C. J.; Shapley, J. R. Catalytic Nitrate and Nitrite Reduction with Pd-Cu/PVP Colloids in Water: Composition, Structure, and Reactivity Correlations. *J. Phys. Chem. C* **2009**, *113*, 8177−8185.

(12) Shin, H.; Jung, S.; Bae, S.; Lee, W.; Kim, H. Nitrite Reduction Mechanism on a Pd Surface. *Environ. Sci. Technol.* **2014**, *48*, 12768−12774.

(13) Zhang, Z.; Shi, W.; Wang, W.; Xu, Y.; Bao, X.; Zhang, R.; Zhang, B.; Guo, Y.; Cui, F. Interfacial Electronic Effects of Palladium Nanocatalysts on the By-Product Ammonia Selectivity during Nitrite Catalytic Reduction. *Environ. Sci. Nano* **2018**, *5*, 338−349.

(14) Brunet Espinosa, R.; Lefferts, L. Ni in CNFs: Highly Active for Nitrite Hydrogenation. *ACS Catal.* **2016**, *6*, 5432−5440.

(15) Leigh, G. J. Haber-Bosch and Other Industrial Processes. In *Catalysts for Nitrogen Fixation*; Springer, 2004; pp 33−54.

(16) Spokas, K. A.; Novak, J. M.; Venterea, R. T. Biochar's Role as an Alternative N-Fertilizer: Ammonia Capture. *Plant Soil* **2012**, *350*, 35−42.

(17) Pelletier, L.; McFarlan, A.; Maffei, N. Ammonia Fuel Cell Using Doped Barium Cerate Proton Conducting Solid Electrolytes. *J. Power Sources* **2005**, *145*, 262−265.

(18) Zamfirescu, C.; Dincer, I. Using Ammonia as a Sustainable Fuel. *J. Power Sources* **2008**, *185*, 459−465.

(19) Erisman, J. W.; Sutton, M. A.; Galloway, J.; Klimont, Z.; Winiwarter, W. How a Century of Ammonia Synthesis Changed the World. *Nat. Geosci.* **2008**, *1*, 636.

(20) Foster, S. L.; Bakovic, S. I. P.; Duda, R. D.; Maheshwari, S.; Milton, R. D.; Minteer, S. D.; Janik, M. J.; Renner, J. N.; Greenlee, L. F. Catalysts for Nitrogen Reduction to Ammonia. *Nat. Catal.* **2018**, *1*, 490.

(21) Singh, A. R.; Rohr, B. A.; Schwalbe, J. A.; Cargnello, M.; Chan, K.; Jaramillo, T. F.; Chorkendorff, I.; Nørskov, J. K. Electrochemical Ammonia Synthesis - The Selectivity Challenge. *ACS Catal.* **2017**, 706−709.

(22) Andersen, S. Z.; Čolić, V.; Yang, S.; Schwalbe, J. A.; Nielander, A. C.; McEnaney, J. M.; Enemark-Rasmussen, K.; Baker, J. G.; Singh, A. R.; Rohr, B. A.; et al. A Rigorous Electrochemical Ammonia Synthesis Protocol with Quantitative Isotope Measurements. *Nature* **2019**, 504−508.

(23) Clark, C. A.; Reddy, C. P.; Xu, H.; Heck, K. N.; Luo, G.; Senftle, T. P.; Wong, M. S. Mechanistic Insights into PH-Controlled Nitrite Reduction to Ammonia and Hydrazine over Rhodium. *ACS Catal.* **2020**, *10*, 494−509.

(24) Chaplin, B. P.; Reinhard, M.; Schneider, W. F.; Schüth, C.; Shapley, J. R.; Strathmann, T. J.; Werth, C. J. Critical Review of Pd-Based Catalytic Treatment of Priority Contaminants in Water. *Environ. Sci. Technol.* **2012**, 3655−3670.

(25) Hörold, S.; Vorlop, K. D.; Tacke, T.; Sell, M. Development of Catalysts for a Selective Nitrate and Nitrite Removal from Drinking Water. *Catal. Today* **1993**, *17*, 21−30.

(26) Dubrovsky, N. M.; Burow, K. R.; Clark, G. M.; Gronberg, J. A. M.; Hamilton, P. A.; Hitt, K. J.; Mueller, D. K.; Munn, M. D.; Nolan, B. T.; Puckett, L. J. et al. *Nutrients in the Nation's Streams and Groundwater, 1992−2004*; US Geological Survey, 2010.

(27) Jordan, T. E.; Whigham, D. F.; Hofmockel, K. H.; Pittek, M. A. Nutrient and Sediment Removal by a Restored Wetland Receiving Agricultural Runoff. *J. Environ. Qual.* **2003**, *32*, 1534−1547.

(28) Huett, D. O.; Morris, S. G.; Smith, G.; Hunt, N. Nitrogen and Phosphorus Removal from Plant Nursery Runoff in Vegetated and Unvegetated Subsurface Flow Wetlands. *Water Res.* **2005**, *39*, 3259−3272.

(29) Headley, T. R.; Huett, D. O.; Davison, L. The Removal of Nutrients from Plant Nursery Irrigation Runoff in Subsurface Horizontal-Flow Wetlands. *Water Sci. Technol.* **2001**, 77−84.

(30) Pintar, A.; Batista, J. Catalytic Stepwise Nitrate Hydrogenation in Batch-Recycle Fixed-Bed Reactors. *J. Hazard. Mater.* **2007**, *149*, 387−398.

(31) Jensen, V. B.; Darby, J. L. Brine Disposal Options for Small Systems in California's Central Valley. *J. - Am. Water Works Assoc.* **2016**, *108*, E276–E289.

(32) Ferrin, P.; Simonetti, D.; Kandoi, S.; Kunkes, E.; Dumesic, J. A.; Nørskov, J. K.; Mavrikakis, M. Modeling Ethanol Decomposition on Transition Metals: A Combined Application of Scaling and Brønsted-Evans-Polanyi Relations. *J. Am. Chem. Soc.* **2009**, *131*, 5809–5815.

(33) Troutman, J. P.; Li, H.; Haddix, A. M.; Kienzle, B. A.; Henkelman, G.; Humphrey, S. M.; Werth, C. J. PdAg Alloy Nanocatalysts: Toward Economically Viable Nitrite Reduction in Drinking Water. *ACS Catal.* **2020**.

(34) Luo, L.; Duan, Z.; Li, H.; Kim, J.; Henkelman, G.; Crooks, R. M. Tunability of the Adsorbate Binding on Bimetallic Alloy Nanoparticles for the Optimization of Catalytic Hydrogenation. *J. Am. Chem. Soc.* **2017**, *139*, 5538–5546.

(35) Guo, H.; Li, H.; Jarvis, K.; Wan, H.; Kunal, P.; Dunning, S. G.; Liu, Y.; Henkelman, G.; Humphrey, S. M. Microwave-Assisted Synthesis of Classically Immiscible Ag–Ir Alloy Nanoparticle Catalysts. *ACS Catal.* **2018**, *8*, 11386–11397.

(36) Guo, H.; Fang, Z.; Li, H.; Fernandez, D.; Henkelman, G.; Humphrey, S. M.; Yu, G. Rational Design of Rhodium–Iridium Alloy Nanoparticles as Highly Active Catalysts for Acidic Oxygen Evolution. *ACS Nano* **2019**, *13*, 13225–13234.

(37) Guo, H.; Li, H.; Fernandez, D.; Willis, S.; Jarvis, K.; Henkelman, G.; Humphrey, S. M. Stabilizer-Free CuIr Alloy Nanoparticle Catalysts. *Chem. Mater.* **2019**, *31*, 10225–10235.

(38) Wang, T.; Li, Y. W.; Wang, J.; Beller, M.; Jiao, H. Dissociative Hydrogen Adsorption on the Hexagonal Mo2C Phase at High Coverage. *J. Phys. Chem. C* **2014**, *118*, 8079–8089.

(39) Kobayashi, H.; Yamauchi, M.; Ikeda, R.; Yamamoto, T.; Matsumura, S.; Kitagawa, H. Double Enhancement of Hydrogen Storage Capacity of Pd Nanoparticles by 20 At% Replacement with Ir; Systematic Control of Hydrogen Storage in Pd-M Nanoparticles (M = Ir, Pt, Au). *Chem. Sci.* **2018**, *9*, 5536–5540.

(40) Fierro, C. Ammonia Adsorption on a Model Pt(111) Surface: A Molecular Orbital Approach. *J. Phys. Chem. A* **1988**, *92*, 4401–4405.

(41) Li, H.; Shin, K.; Henkelman, G. Effects of Ensembles, Ligand, and Strain on Adsorbate Binding to Alloy Surfaces. *J. Chem. Phys.* **2018**, *149*, No. 174705.

(42) D'Arino, M.; Pinna, F.; Strukul, G. Nitrate and Nitrite Hydrogenation with Pd and Pt/SnO2 Catalysts: The Effect of the Support Porosity and the Role of Carbon Dioxide in the Control of Selectivity. *Appl. Catal., B* **2004**, *53*, 161–168.

(43) Marchesini, F. A.; Irusta, S.; Querini, C.; Miró, E. Spectroscopic and Catalytic Characterization of Pd-In and Pt-In Supported on Al2O3 and SiO2, Active Catalysts for Nitrate Hydrogenation. *Appl. Catal., A* **2008**, *348*, 60–70.

(44) Prüsse, U.; Vorlop, K. D. Supported Bimetallic Palladium Catalysts for Water-Phase Nitrate Reduction. *J. Mol. Catal. A: Chem.* **2001**, *46*, 3655–3670.

(45) Chinthaginjala, J. K.; Lefferts, L. Support Effect on Selectivity of Nitrite Reduction in Water. *Appl. Catal., B* **2010**, *101*, 144–149.

(46) García, S.; Zhang, L.; Piburn, G. W.; Henkelman, G.; Humphrey, S. M. Microwave Synthesis of Classically Immiscible Rhodium-Silver and Rhodium-Gold Alloy Nanoparticles: Highly Active Hydrogenation Catalysts. *ACS Nano* **2014**, *8*, 11512–11521.

(47) Li, H.; Chai, W.; Henkelman, G. Selectivity for Ethanol Partial Oxidation: The Unique Chemistry of Single-Atom Alloy Catalysts on Au, Ag, and Cu(111). *J. Mater. Chem. A* **2019**, *7*, 23868–23877.

(48) Gilroy, K. D.; Ruditskiy, A.; Peng, H. C.; Qin, D.; Xia, Y. Bimetallic Nanocrystals: Syntheses, Properties, and Applications. *Chem. Rev.* **2016**, *116*, 10414–10472.

(49) García-Hernández, M.; López, N.; Moreira, I. D. P. R.; Paniagua, J. C.; Illas, F. Ab Initio Cluster Model Approach to the Chemisorption of NH3 on Pt(111). *Surf. Sci.* **1999**, *430*, 18–28.

(50) Mavrikakis, M.; Hammer, B.; Nørskov, J. Effect of Strain on the Reactivity of Metal Surfaces. *Phys. Rev. Lett.* **1998**, *81*, 2819–2822.

(51) Liu, P.; Nørskov, J. K. Ligand and Ensemble Effects in Adsorption on Alloy Surfaces. *Phys. Chem. Chem. Phys.* **2001**, *3*, 3814–3818.

(52) Fernndez, E. M.; Moses, P. G.; Toftelund, A.; Hansen, H. A.; Martínez, J. I.; Abild-Pedersen, F.; Kleis, J.; Hinnemann, B.; Rossmeisl, J.; Bligaard, T.; et al. Scaling Relationships for Adsorption Energies on Transition Metal Oxide, Sulfide, and Nitride Surfaces. *Angew. Chem., Int. Ed.* **2008**, *47*, 4683–4686.

(53) Hammer, B.; Norskov, J. K. Why Gold Is the Noblest of All the Metals. *Nature* **1995**, *376*, 238.